PHYSICAL REVIEW A VOLUME 18, NUMBER 1 JULY 1978

Bethe cross sections for the sodium isoelectronic sequence

Yong-Ki Kim and Kwok-tsang Cheng
Argonne National Laboratory, Argonne, Illinois 60439
(Received 7 March 1978)

Bethe cross sections for the excitation of Na-like ions to the $3^2P_{1/2}$, $3^2P_{3/2}$, $4^2P_{1/2}$, and $4^2P_{3/2}$ states from the ground state are computed from the relativistic Hartree-Fock wave functions. As the nuclear charge is increased, excitation cross sections to the $^2P_{3/2}$ states are affected far more by relativistic effects than those to the $^2P_{1/2}$ states. The asymptotic ionization cross sections for the neutral Na atom and Fe^{15+} ion are computed from a sum rule, i.e., by subtracting the sum of discrete excitation cross sections from the total inelastic-scattering cross section obtained from the sum rule. The ionization cross sections thus obtained are

$$\sigma_{\text{ion}}(\text{Na}) = \beta^{-2}(2.51\{\ln[\beta^2/(1-\beta^2)] - \beta^2\} + 26.3) \times 10^{-20}\ \text{cm}^2,$$
$$\sigma_{\text{ion}}(\text{Fe}^{15+}) = \beta^{-2}(0.209\ \{\ln[\beta^2/(1-\beta^2)] - \beta^2\} + 1.64) \times 10^{-20}\ \text{cm}^2,$$

where β is the incident electron or proton speed divided by that of light. The cross section for Na is in agreement with that calculated by McGuire, but not with the electron-impact experiment by McFarland and Kinney. The ionization cross section for Fe^{15+} is a factor of 2 to 3 larger than the Coulomb-Born results by Rudge and Schwartz and by Bely in the asymptotic region.

I. INTRODUCTION

Cross sections for discrete excitations and ionization by electron impact of highly stripped ions are of great interest in the diagnosis of hot plasma, as well as in estimating the energy loss in fusion devices through impurity ions.[1] To study systematic trends of such cross sections along an isoelectronic sequence, we calculated the Bethe cross sections for the resonance transitions of Na-like ions. It is well known that the Coulomb attraction of an ion produces a threshold behavior entirely different from that predicted by the plane-wave Born approximation (PWBA); for a given energy transfer, the cross section based on the Coulomb-Born approximation (CBA) starts at a finite value, whereas the PWBA cross section starts at zero.[2] In spite of this defect of the PWBA at the threshold, the CBA cross sections merge into the PWBA cross sections at high incident energies. Since the Bethe approximation embodies correct high-energy behavior of the PWBA,[3] the Bethe cross sections serve as the asymptotic limit for the CBA cross sections. In the CBA, many partial waves are needed as incident energy is increased. On the contrary, the Bethe cross section is simple to evaluate, and becomes very reliable for high incident energies. Since the Bethe cross section for a given transition is expressed in terms of one or two parameters for arbitrary (but high) incident energies, it is well suited for use in various modeling studies, such as the one for power loss by impurities in Tokamak devices.[4] Furthermore, since the Bethe cross section for an incident electron is the same as that for a proton of the same speed, the Bethe parameters presented here can also be used for fast protons.

A sum rule exists for the Bethe cross sections,[3,5] and reliable ionization cross sections can be obtained by subtracting the sum of discrete excitation cross sections from the total inelastic-scattering cross section calculated by the sum rule.[6] We calculated additional Bethe cross sections for excitations of the neutral Na and the Fe^{15+} ion to higher discrete states and evaluated the ionization cross sections by the sum-rule method, which avoids direct computation of continuum wave functions—a common source of numerical difficulty as incident energy increases. Many papers have been published on the ionization cross section for Na, both experimental and theoretical,[7-14] but agreement among them is poor. Our result clearly supports one of the theoretical results.

Relevant formulas and notations are introduced in Sec. II, and the Bethe cross sections for the resonance transitions are presented in Sec. III. The ionization cross sections are discussed in Sec. IV, and our results are compared with available theoretical and experimental data in Sec. V.

II. THEORY

In the Born approximation, the generalized oscillator strength (GOS) plays a central role. For the excitation of an atom from its ground state $|0\rangle$ to an excited state $|n\rangle$ by a fast electron of speed v, the GOS is defined as[5]

$$f_n(K) = \frac{E_n}{R}\,\frac{|\langle n|\sum_j e^{i\vec{K}\cdot\vec{r}_j}|0\rangle|^2}{(Ka_0)^2}, \tag{1}$$

 © 1978 The American Physical Society

where $\vec{K}\hbar$ is the momentum transfer, E_n is the excitation energy, $\vec{r}_j$ is the position vector of the jth electron in the ion, a_0 is the Bohr radius, and R is the Rydberg energy. The integrated Born cross section σ_n^B is given by

$$\sigma_n^B = \frac{4\pi a_0^2}{T/R}\frac{R}{E_n}\int_{(K_{\min}a_0)^2}^{(K_{\max}a_0)^2} f_n(K)\, d\ln(Ka_0)^2 , \qquad (2)$$

where $T=\frac{1}{2}mv^2$, with m being the mass of the electron, and where $K_{\max}$ and $K_{\min}$ are the limits of the momentum transfer determined from the kinematics. The limits are given by

$$(K_{\min}a_0)^2 \approx E_n^2/4TR \equiv Q_{\min} \qquad (3a)$$

and

$$(K_{\max}a_0)^2 \approx 4TM^2/Rm^2 \equiv Q_{\max}, \qquad (3b)$$

where M is the mass of the incident particle.

The Bethe cross section σ_n is the leading part of an asymptotic expansion of σ_n^B. It is given in terms of two parameters A_n and B_n as[3,5]

$$\sigma_n = \frac{4\pi a_0^2}{T/R}\left[A_n \ln\left(\frac{T}{R}\right)+B_n\right]. \qquad (4)$$

The Bethe approximation prescribes a definite procedure to find a cutoff parameter Q_0 between $Q_{\min}$ and $Q_{\max}$ such that the integral in Eq. (2) can be approximated by the area of a rectangle of height A_n and width $\ln(Q_0/Q_{\min})$.[3,5] Both A_n and Q_0 depend on the GOS only. In fact, A_n is given by

$$A_n \equiv f_n R/E_n = \left|\left\langle n\left|\sum_j \vec{r}_j\right|0\right\rangle\right|^2 \Big/ 3a_0^2 , \qquad (5)$$

where the optical oscillator strength f_n is obtained from the GOS in the limit $K\to 0$. The second Bethe parameter in Eq. (4) is given by

$$B_n = A_n \ln(4Q_0R^2/E_n^2) , \qquad (6)$$

where B_n depends on the excitation energy E_n, as well as on the shape of the GOS through Q_0. Note that, for dipole-forbidden transitions, A_n vanishes because $f_n=0$; in that case, B_n is given by[5]

$$B_n = \int_0^\infty \frac{f_n(K)}{E_n/R}\, d\ln(Ka_0)^2 . \qquad (7)$$

The Bethe cross sections can be summed over for all excitations (including ionization) to produce the total cross section for inelastic scattering[5] in the same form as Eq. (4)

$$\sigma_{\text{tot}} \equiv \sum_n \sigma_n = \frac{4\pi a_0^2}{T/R}\left[A_{\text{tot}}\ln\left(\frac{T}{R}\right)+B_{\text{tot}}\right]. \qquad (8)$$

(Hereafter, we use $\sum_n$ to denote the sum over both discrete and continuum states.) The constants A_{tot} and B_{tot} are calculated from the ground-state wave function and moments of the dipole-oscillator strength distribution. The first constant is given by[5]

$$A_{\text{tot}} = \sum_n f_n \frac{R}{E_n} = \left\langle 0\left|\left(\sum_j \vec{r}_j\right)^2\right|0\right\rangle \Big/ 3a_0^2 . \qquad (9)$$

The second constant is

$$B_{\text{tot}} = -2L(-1)+I_1-I_2+A_{\text{tot}}\ln 4 , \qquad (10)$$

where

$$L(-1) = \sum_n \left(\frac{f_nR}{E_n}\right)\ln\left(\frac{E_n}{R}\right), \qquad (11)$$

and I_1 and I_2 are integrals defined in terms of the ground-state wave function. Explicit formulas for I_1 and I_2 are given in Ref. 5. The moment $L(-1)$, however, cannot be evaluated from the ground-state wave function alone; one must deduce it from either experimental or theoretical f values, including those for the continuum transitions.

After the Bethe parameters for discrete transitions are calculated for lower members of a Rydberg series, one can extrapolate them to higher members of the series by scaling according to quantum defects.[15] Then, one can sum σ_n for all discrete transitions below the first ionization threshold

$$\sigma_{\text{ex}} = \sum_{\text{discrete}} \sigma_n , \qquad (12)$$

and obtain the ionization cross section σ_{ion} by subtraction

$$\sigma_{\text{ion}} = \sigma_{\text{tot}} - \sigma_{\text{ex}} . \qquad (13)$$

The ionization cross section obtained through Eq. (13) includes all inner-shell excitations that eventually produce ions.

For very fast incident electrons ($T>5$ keV), relativistic forms of Eqs. (4) and (8) should be used[16]

$$\sigma_n = \frac{4\pi a_0^2\alpha^2}{\beta^2}\left\{A_n\left[\ln\left(\frac{\beta^2}{1-\beta^2}\right)-\beta^2\right]+C_n\right\}, \qquad (14)$$

and

$$\sigma_{\text{tot}} = \frac{4\pi a_0^2\alpha^2}{\beta^2}\left\{A_{\text{tot}}\left[\ln\left(\frac{\beta^2}{1-\beta^2}\right)-\beta^2\right]+C_{\text{tot}}\right\}, \qquad (15)$$

where α is the fine-structure constant, $\beta=v/c$ with the speed of light c, and for both C_n and C_{tot},

$$C = B - 2A\ln\alpha . \qquad (16)$$

III. BETHE CROSS SECTIONS FOR THE Na SEQUENCE

We calculated A_n and B_n for excitations to the $3\,^2P_{1/2,3/2}$ and $4\,^2P_{1/2,3/2}$ states from the ground state $3\,^2S_{1/2}$ for selected members of the Na isoelectronic sequence from the relativistic Hartree-Fock (HF) wave functions.[17] Since there is only one valence electron in Na-like ions, the HF

TABLE I. Bethe parameters for the $3\,^2S \rightarrow 3\,^2P$, $4\,^2P$ transitions of Na-like ions.

Ion	Z	n	E_n (Ry)	A_n	B_n	Ion	Z	n	E_n (Ry)	A_n	B_n
Na	11	$3\,^2P_{1/2}$	1.434(−1) [a]	2.26	6.03	Kr^{25+}	36	$3\,^2P_{1/2}$	4.179	2.07(−2)	1.76(−2)
		$3\,^2P_{3/2}$	1.435(−1)	4.52	1.20(+1)			$3\,^2P_{3/2}$	5.126	4.21(−2)	1.82(−2)
		$4\,^2P_{1/2}$	2.637(−1)	1.65(−2)	2.07(−1)			$4\,^2P_{1/2}$	4.264(+1)	2.33(−3)	−1.16(−2)
		$4\,^2P_{3/2}$	2.637(−1)	3.36(−2)	4.15(−1)			$4\,^2P_{3/2}$	4.301(+1)	4.10(−3)	−2.05(−2)
Mg^+	12	$3\,^2P_{1/2}$	3.153(−1)	1.01	2.08	Mo^{31+}	42	$3\,^2P_{1/2}$	5.221	1.40(−2)	1.11(−2)
		$3\,^2P_{3/2}$	3.161(−1)	2.01	4.15			$3\,^2P_{3/2}$	7.183	2.86(−2)	3.97(−3)
		$4\,^2P_{1/2}$	7.168(−1)	1.41(−4)	4.75(−2)			$4\,^2P_{1/2}$	6.260(+1)	1.73(−3)	−9.21(−3)
		$4\,^2P_{3/2}$	7.171(−1)	2.23(−4)	9.60(−2)			$4\,^2P_{3/2}$	6.336(+1)	2.91(−3)	−1.57(−2)
Al^{2+}	13	$3\,^2P_{1/2}$	4.811(−1)	6.09(−1)	1.08	Xe^{43+}	54	$3\,^2P_{1/2}$	7.495	7.47(−3)	5.10(−3)
		$3\,^2P_{3/2}$	4.832(−1)	1.22	2.15			$3\,^2P_{3/2}$	1.381(+1)	1.56(−2)	−8.77(−3)
		$4\,^2P_{1/2}$	1.288	3.03(−3)	1.24(−2)			$4\,^2P_{1/2}$	1.149(+2)	1.04(−3)	−6.15(−3)
		$4\,^2P_{3/2}$	1.289	5.74(−3)	2.59(−2)			$4\,^2P_{3/2}$	1.174(+2)	1.55(−3)	−9.32(−3)
P^{4+}	15	$3\,^2P_{1/2}$	8.038(−1)	3.07(−1)	4.50(−1)	W^{63+}	74	$3\,^2P_{1/2}$	1.215(+1)	3.36(−3)	1.67(−3)
		$3\,^2P_{3/2}$	8.110(−1)	6.15(−1)	8.89(−1)			$3\,^2P_{3/2}$	3.960(+1)	7.30(−3)	−1.40(−2)
		$4\,^2P_{1/2}$	2.749	6.42(−3)	−1.14(−2)			$4\,^2P_{1/2}$	2.443(+2)	5.31(−4)	−3.51(−3)
		$4\,^2P_{3/2}$	2.752	1.23(−2)	−2.13(−2)			$4\,^2P_{3/2}$	2.555(+2)	5.74(−4)	−3.92(−3)
Ar^{7+}	18	$3\,^2P_{1/2}$	1.278	1.54(−1)	1.90(−1)	Au^{68+}	79	$3\,^2P_{1/2}$	1.356(+1)	2.83(−3)	1.27(−3)
		$3\,^2P_{3/2}$	1.302	3.08(−1)	3.69(−1)			$3\,^2P_{3/2}$	5.104(+1)	6.22(−3)	−1.41(−2)
		$4\,^2P_{1/2}$	5.702	6.75(−3)	−1.99(−2)			$4\,^2P_{1/2}$	2.864(+2)	4.58(−4)	−3.10(−3)
		$4\,^2P_{3/2}$	5.711	1.29(−2)	−3.81(−2)			$4\,^2P_{3/2}$	3.018(+2)	4.42(−4)	−3.10(−3)
Fe^{15+}	26	$3\,^2P_{1/2}$	2.540	4.94(−2)	4.89(−2)	Th^{79+}	90	$3\,^2P_{1/2}$	1.703(+1)	1.97(−3)	6.70(−4)
		$3\,^2P_{3/2}$	2.730	9.95(−2)	8.37(−2)			$3\,^2P_{3/2}$	8.795(+1)	4.46(−3)	−1.35(−2)
		$4\,^2P_{1/2}$	1.800(+1)	4.20(−3)	−1.74(−2)			$4\,^2P_{1/2}$	3.961(+2)	3.38(−4)	−2.39(−3)
		$4\,^2P_{3/2}$	1.808(+1)	7.82(−3)	−3.25(−2)			$4\,^2P_{3/2}$	4.252(+2)	2.35(−4)	−1.73(−3)

[a] Numbers in parentheses denote powers of ten, e.g., $1.434(-1) = 1.434\times 10^{-1}$.

model is expected to work well. Conclusions drawn from our work on cross sections are unlikely to be affected by uncertainties in wave functions.

The Bethe parameters and excitation energies are presented in Table I. In Figs. 1–3, we compare the Bethe parameters computed from the relativistic and nonrelativistic Hartree-Fock wave functions for the $3\,^2P_{1/2}$, $3\,^2P_{3/2}$, and $4\,^2P_{1/2}$ transitions, respectively. The Bethe parameters were scaled by Z^2, where Z is the nuclear charge. We find that both Z^2A_n and Z^2B_n become more or less constant for $Z > 30$.

The definition of A_n [Eq. (5)] suggests that it scales as Z^{-2} in the hydrogenic case, but, for the Na sequence, it is not at all clear whether A_n should scale according to the nuclear charge or the screened charge $\zeta = Z - 10$. In fact, Rudge and Schwartz[18] scale ionization cross sections by the square of ionization potentials. To select a suitable scaling variable, we multiplied A_n by Z^2, ζ^2, E_n, and E_n^2 for the $4\,^2P_{3/2}$ transition.

The scaled results are presented in Fig. 4. The reduction of the relativistic A_n for high Z in Figs. 4(a)–4(c) is caused by the decrease of the transition matrix element $|\langle n|\vec{r}|0\rangle|^2$ as Z increases. Figures 1–3 and the nonrelativistic result in Fig. 4(a) clearly demonstrate that the Z^2 scaling is preferred. The relativistic and nonrelativistic values of Z^2B_n for the $4\,^2P_{3/2}$ transition also show a wide disagreement (Fig. 5). The differences in the relativistic and nonrelativistic values of B_n for the

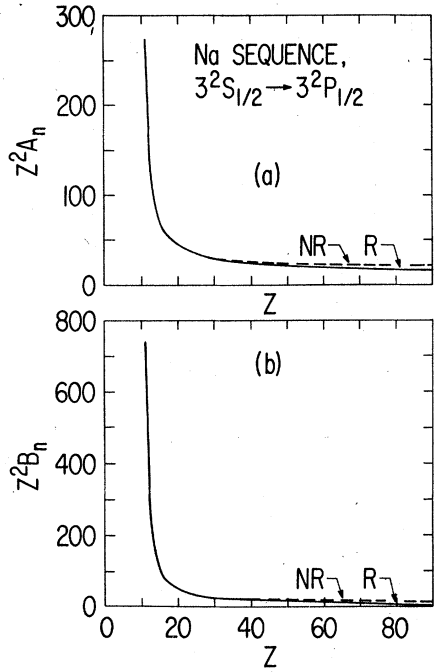

FIG. 1. The Bethe parameters for the $3^2P_{1/2}$ excitation of Na-like ions as functions of nuclear charge Z. The solid curves marked R represent values calculated from the relativistic Hartree-Fock wave functions, and the broken curves marked NR those from the nonrelativistic Hartree-Fock wave functions. See Eqs. (4)–(7) for definitions of A_n and B_n.

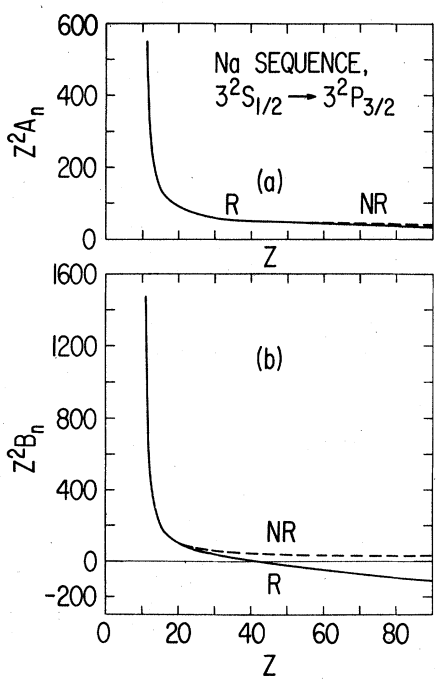

FIG. 2. The Bethe parameters for the $3\,^2P_{3/2}$ excitation of Na-like ions. See Fig. 1 for legends.

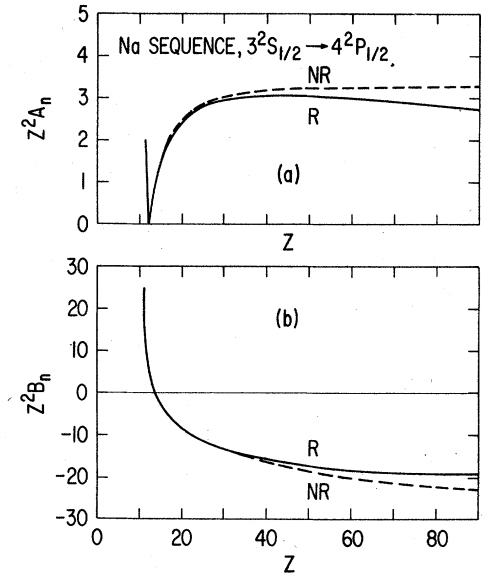

FIG. 3. The Bethe parameters for the $4\,^2P_{1/2}$ excitation of Na-like ions. See Fig. 1 for legends. The sharp dip in (a) at $Z=12$ comes from the Cooper minimum in f value.

$3\,^2P_{3/2}$ and $4\,^2P_{3/2}$ transitions arise for different reasons. As is illustrated in Figs. 6 and 7, the integrated Born cross section σ_n^B is given (aside from a trivial constant) by the area bounded by the $f_n(K)/E_n$ curve and appropriate limits of the momentum transfer [see Eq. (2)]. The lower limit Q_{min} is a function of the incident energy and the excitation energy; but the upper limit Q_{max} for fast incident particles can be replaced by infinity with-

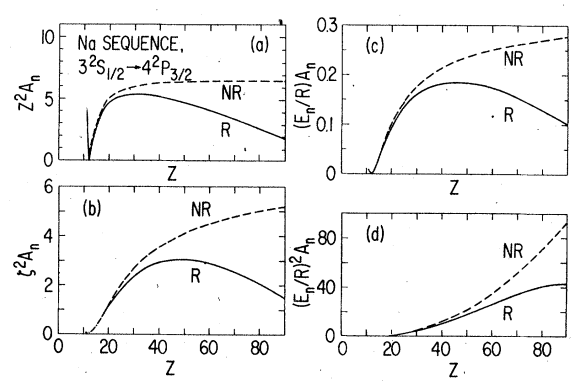

FIG. 4. Scaling of the Bethe parameter A_n for the $4\,^2P_{3/2}$ excitation of Na-like ions. The screened charge ζ is defined as $\zeta = Z - 10$, and E_n/R is the excitation energy in Ry. See Fig. 1 for other legends. The similarity between plots (b) and (c) results from the approximate scaling of E_n as ζ^2. The dip in (a) at $Z=12$ comes from the Cooper minimum in f value.

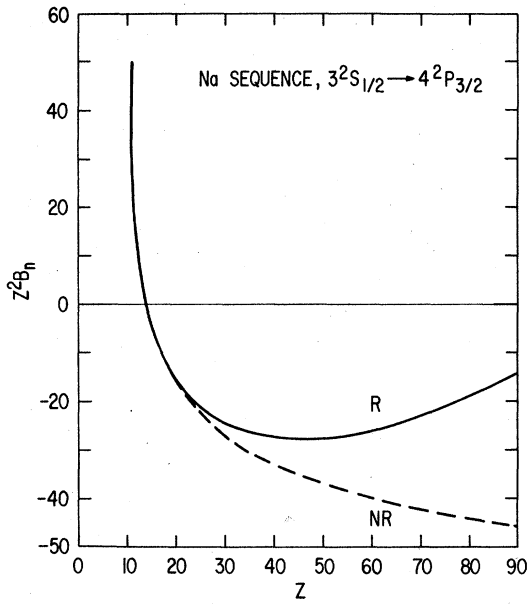

FIG. 5. The Bethe parameter B_n for the $4\,^2P_{3/2}$ excitation of Na-like ions. See Fig. 1 for legends.

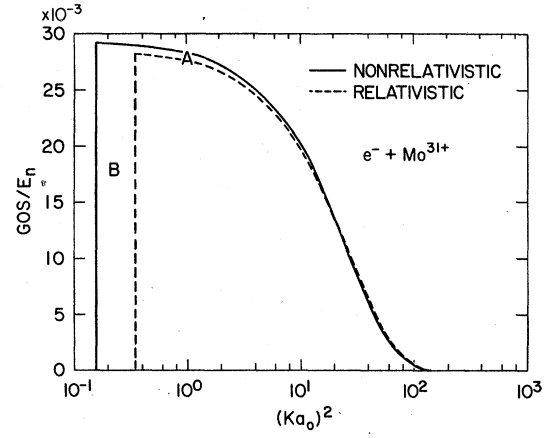

FIG. 6. The generalized oscillator strength (GOS) for the $3^2P_{3/2}$ excitation of Mo^{31+} as a function of momentum transfer K in a.u. The GOS is divided by the excitation energy (E_n in Ry) so that the areas bound by solid and broken lines are proportional to the Born cross sections (σ^B) for the excitation by a 500-eV incident electron. Area A represents the change in σ^B by relativistic contraction of the Mo^{31+} orbitals, and area B the change in σ^B due to the shift in the lower limit of K resulting from the relativistic increase of E_n.

out loss of numerical accuracy [see Eq. (4)].[6] For the $3\,^2P_{3/2}$ transition, a large change in E_n from relativistic effects is directly responsible for a large change in $Q_{\min}$ and, hence, in B_n; this change is represented by the area B in Fig. 6. For the $4\,^2P_{3/2}$ transition, the matrix element $|\langle 4p|\vec{r}|3s\rangle|^2$ in Eq. (5) is reduced by relativistic effects resulting in a lower height of the relativistic curve in Fig. 7; the relativistic change in B_n

TABLE II. Bethe parameters for the allowed transitions of Na.

n	E_n (Ry)	A_n	B_n	f_n
		(a) Transitions to the $n\,^2P_{1/2}$ states		
5	3.065(−1)[a]	2.10(−3)	5.32(−2)	6.44(−4)
6	3.268(−1)	5.97(−4)	2.23(−2)	1.95(−4)
7	3.380(−1)	2.47(−4)	1.17(−2)	8.34(−5)
$n \geq 8$, Eq. (17)				
a		3.89(−2)	2.18	1.20(−2)
b		−3.12(−1)	1.46(+1)	2.94(−2)
c		3.88(+1)	2.37(+2)	9.73
Quantum defect	$\delta = 0.8384$			
Sum $n \geq 3$		2.28	6.35	0.334
		(b) Transitions to the $n\,^2P_{3/2}$ states		
5	3.065(−1)	4.31(−3)	1.07(−1)	1.32(−3)
6	3.268(−1)	1.23(−3)	4.49(−2)	4.04(−4)
7	3.380(−1)	5.12(−4)	2.35(−2)	1.73(−4)
$n \geq 8$, Eq. (17)				
a		8.08(−2)	4.39	2.49(−2)
b		−5.92(−1)	2.93(+1)	7.23(−2)
c		7.87(+1)	4.77(+2)	1.97(+1)
Quantum defect	$\delta = 0.8384$			
Sum $n \geq 3$		4.57	12.68	0.669

[a]Numbers in parentheses denote powers of ten.

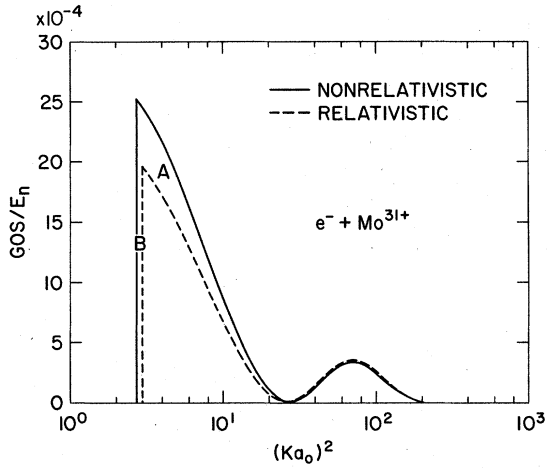

FIG. 7. The generalized oscillator strength for the $4\,^2P_{3/2}$ excitation of Mo^{31+}. The areas bound by the curves are proportional to the Born cross section for a 5-keV incident electron. See Fig. 6 for other legends.

comes mostly from area A in Fig. 7.

To compute σ_{ion} by the sum rule [Eq. (13)], we evaluated the Bethe parameters for additional excitations for the neutral Na and Fe^{15+} ion. To extrapolate the Bethe parameters for higher members of a Rydberg series, we used a three-term formula

$$A_n = a(n^*)^{-3} + b(n^*)^{-5} + c(n^*)^{-7}, \qquad (17)$$

where $n^* = n - \delta$ is the effective quantum number, and δ is the quantum defect. To be consistent with other theoretical data for the cross sections, we have also used theoretical term values to determine δ. Our values for the ^2S and ^2P series in Na ($\delta_s = 1.32$ and $\delta_p = 0.84$) are in excellent agreement with those obtained from experimental energy levels ($\delta_s = 1.35$ and $\delta_p = 0.85$). The agreement between the theoretical and experimental δ for ^2D and higher series is poor, but the difference hardly affects the sum of the cross sections because δ for these series is small (<0.02). Another formula of the same form as Eq. (17) was used for B_n. The additional Bethe parameters of Na are listed in Tables II and III.

As expected, for Na, spin-orbit splitting introduces a barely noticeable departure from the statistical ratio only in the ^2P series (Table II). For this reason, we only present sums of $j = l \pm \frac{1}{2}$ series for a given l in Table III. The Bethe parameters for additional transitions of Fe^{15+} are given in Tables IV and V. We see a slight departure from the statistical ratio in the Bethe parameters up to the ^2F series, but not in the ^2G series.

One aspect of a shift toward hydrogenic behavior as Z increases is the sum of f values for the

TABLE III. Bethe parameters for the forbidden transitions of Na.

n	E_n (Ry)	B_n
(a) Transitions to the $n\,^2S_{1/2}$ states ($A_n \equiv 0$)		
4	2.240(−1) [a]	6.50(−1)
5	2.902(−1)	1.29(−1)
6	3.186(−1)	4.94(−2)
7	3.333(−1)	2.46(−2)
$n \geq 8$, Eq. (17)		
a		3.66
b		1.94(+1)
c		2.40(+2)
Quantum defect	$\delta = 1.324$	
Sum $n \geq 4$		9.04(−1)
(b) Sum of transitions to the $n\,^2D_{3/2}$ and $n\,^2D_{5/2}$ states ($A_n \equiv 0$)		
3	2.530(−1)	1.24
4	3.017(−1)	3.17(−1)
5	3.243(−1)	1.31(−1)
6	3.365(−1)	6.76(−2)
7	3.439(−1)	3.98(−2)
$n \geq 8$, Eq. (17)		
a		1.14(+1)
b		9.34(+1)
c		7.12(+2)
Quantum defect	$\delta = 0.0053$	
Sum $n \geq 3$		1.905
(c) Sum of transitions to the $n\,^2F_{5/2}$ and $n\,^2F_{7/2}$ states ($A_n \equiv 0$)		
4	3.018(−1)	4.05(−2)
5	3.243(−1)	2.42(−2)
6	3.366(−1)	1.46(−2)
7	3.439(−1)	9.33(−3)
$n \geq 8$, Eq. (17)		
a		3.22
b		3.30
c		−2.01(+2)
Quantum defect	$\delta = 0.0001$	
Sum $n \geq 4$		0.117
(d) Sum of transitions to the $n\,^2G_{7/2}$ and $n\,^2G_{9/2}$ states ($A_n \equiv 0$)		
5	3.243(−1)	8.84(−4)
6	3.366(−1)	8.12(−4)
7	3.439(−1)	6.24(−4)
$n \geq 7$, Eq. (17)		
a		3.20(−1)
b		−5.15
c		−2.24
Quantum defect	$\delta = 0$	
Sum $n \geq 5$		4.75(−3)

[a] Numbers in parentheses denote powers of ten.

TABLE IV. Bethe parameters for the allowed transitions of Fe^{15+}.

n	E_n (Ry)	A_n	B_n	f_n
		(a) Transitions to the $n\,^2P_{1/2}$ states		
5	2.473(+1)[a]	9.32(−4)	−3.84(−3)	2.31(−2)
6	2.827(+1)	3.71(−4)	−1.52(−3)	1.05(−2)
7	3.036(+1)	1.90(−4)	−7.79(−4)	5.76(−3)
$n \geq 8$, Eq. (17)				
a		4.56(−2)	−1.87(−1)	1.42
b		−1.25(−2)	8.30(−2)	1.12(+1)
c		2.99(+1)	−1.24(+2)	3.48(+2)
Quantum defect	$\delta = 0.214$			
Sum $n \geq 3$		5.55(−2)	2.36(−2)	2.55(−1)
		(b) Transitions to the $n\,^2P_{3/2}$ states		
5	2.477(+1)	1.77(−3)	−7.33(−3)	4.39(−2)
6	2.829(+1)	7.10(−4)	−2.93(−3)	2.01(−2)
7	3.038(+1)	3.65(−4)	−1.50(−3)	1.11(−2)
$n \geq 8$, Eq. (17)				
a		8.75(−2)	−3.61(−1)	2.74
b		2.88(−2)	−6.71(−2)	2.00(+1)
c		5.59(+1)	−2.33(+2)	6.41(+2)
Quantum defect	$\delta = 0.206$			
Sum $n \geq 3$		1.11(−1)	3.59(−2)	5.16(−1)

[a] Number in parentheses are powers of ten.

discrete excitations. As is shown in Tables II and IV, the sum

$$f_{ex} = \sum_{\text{discrete}} f_n$$

for Na is 1.00, whereas that for Fe^{15+} is 0.771. The value of $\sum_{n \geq 4} f_n$ for the hydrogen atom[19] is 0.748.

IV. IONIZATION CROSS SECTIONS OF Na AND Fe^{15+}

Both σ_{ex} and σ_{ion} can be expressed in the same form as Eqs. (8) and (15). The Bethe parameters A, B, and C for σ_{tot}, σ_{ex}, and σ_{ion} of Na are presented in Table VI. To calculate B_{tot}, we used $L(-1) = -9.65$ and $I_1 - I_2 = -7.75$. The moment $L(-1)$ is obtained from Ref. 20 and is calculated directly from a weighted sum of f values [see Eq. (11)] using nonrelativistic Herman-Skillman (HS) wave functions. We calculated $I_1 - I_2$ from the relativistic HF wave function. The HS wave function for Na gives[20] $A_{tot} = 7.58$, as compared to the relativistic HF value of 8.19.

For Fe^{15+}, we used $L(-1) = 0.657$ again from the HS wave functions,[21] and $I_1 - I_2 = 0.876$ from the relativistic HF wave function. The HS value[21] of $A_{tot} = 0.275$ compares well with the relativistic HF value of 0.278. Resulting Bethe parameters for σ_{tot}, σ_{ex}, and σ_{ion} of Fe^{15+} are listed in Table VII.

No reliable theoretical method has been developed to evaluate $L(-1)$ directly from relativistic f values. We expect that the uncertainty in the values of $L(-1)$ used in the present work is of the order of 10% in view of the agreement between the HS and relativistic HF values of A_{tot}, a quantity closely related to $L(-1)$.

V. DISCUSSION

A. $3\,^2P$ transition

Before we compare our ionization cross sections with data available in the literature, it is desirable to check the reliability of the PWBA cross sections for the discrete excitations. Fortunately, both the angular distribution of scattered electrons and integrated cross sections for the $3\,^2P$ transition are available for Na. The former tests the GOS [Eq. (1)], and the latter tests σ_n [Eq. (4)]. In Fig. 8 we compare the "experimental" GOS deduced from the angular distribution of the 100- and 150-eV incident electrons by Shuttleworth *et al.*,[22] with our theoretical GOS. The theoretical GOS is the sum of those for the $3\,^2P_{1/2}$ and $3\,^2P_{3/2}$ transitions. We find a close agreement between experiment and theory. The data in Fig. 8

TABLE V. Bethe parameters for the forbidden transitions of Fe^{15+}.

(a) Transitions to the $n\,^2S_{1/2}$ states ($A_n \equiv 0$)

n	E_n (Ry)	B_n
4	1.700(+1) [a]	1.42(−2)
5	2.424(+1)	2.69(−3)
6	2.800(+1)	1.02(−3)
7	3.019(+1)	5.09(−4)
$n \geq 8$, Eq. (17)		
a		1.21(−1)
b		−5.38(−1)
c		8.64(+1)
Quantum defect	$\delta = 0.317$	
Sum $n \geq 4$		1.97(−2)

(b) Transitions to the $n\,^2D_{3/2}$ and $n\,^2D_{5/2}$ states ($A_n \equiv 0$)

	$n\,^2D_{3/2}$		$n\,^2D_{5/2}$	
n	E_n (Ry)	B_n	E_n (Ry)	B_n
3	6.174	1.78(−2)	6.199	2.67(−2)
4	1.934(+1)	4.96(−3)	1.935(+1)	7.39(−3)
5	2.538(+1)	1.43(−3)	2.539(+1)	2.14(−3)
6	2.864(+1)	6.20(−4)	2.864(+1)	9.28(−4)
7	3.059(+1)	3.31(−4)	3.059(+1)	4.95(−4)
$n \geq 8$, Eq. (17)				
a		8.02(−2)		1.20(−1)
b		6.24(−1)		9.32(−1)
c		3.85(+1)		5.74(+1)
Quantum defect	$\delta = 0.073$		$\delta = 0.072$	
Sum $n \geq 3$		2.59(−2)		3.89(−2)

(c) Transitions to the $n\,^2F_{5/2}$ and $n\,^2F_{7/2}$ states ($A_n \equiv 0$)

	$n\,^2F_{5/2}$		$n\,^2F_{7/2}$	
n	E_n (Ry)	B_n	E_n (Ry)	B_n
4	1.988(+1)	5.26(−3)	1.989(+1)	7.01(−3)
5	2.565(+1)	1.00(−3)	2.566(+1)	1.34(−3)
6	2.879(+1)	3.66(−4)	2.879(+1)	4.89(−4)
7	3.068(+ 1)	1.80(−4)	3.069(+1)	2.40(−4)
$n \geq 8$, Eq. (17)				
a		5.25(−2)		7.03(−2)
b		−9.91(−1)		−1.33
c		6.95(+1)		9.28(+1)
Quantum defect	$\delta = 0.009$		$\delta = 0.008$	
Sum $n \geq 4$		7.25(−3)		9.68(−3)

(d) Sum of transitions to the $n\,^2G_{7/2}$ and $n\,^2G_{9/2}$ states ($A_n \equiv 0$)

n	E_n (Ry)	B_n
5	2.568(+1)	1.40(−3)
6	2.881(+1)	7.85(−4)
7	3.070(+1)	4.61(−4)
$n \geq 8$, Eq. (17)		
a		9.41(−2)
b		4.32
c		−5.78(+1)
Quantum defect	$\delta = 0.001$	
Sum $n \geq 5$		3.76(−3)

[a] Numbers in parentheses are powers of ten.

TABLE VI. Bethe parameters for total inelastic scattering, discrete excitation, and ionization cross sections of Na.

	A	B	C
Total inelastic scattering (σ_{tot})	8.19	22.80	103.4
Sum of discrete excitations (σ_{ex})	6.85	21.96	89.4
Ionization (σ_{ion})	1.34	0.84	14.0

indicate that the integrated cross section, which is proportional to the area under the curve, is within 10% of the experimental σ_n at $T > 100$ eV. In Fig. 9 we compare our PWBA result and an electron-impact experiment by Enemark and Gallagher[23] renormalized to our Born result at $T \approx 1$ keV. (The renormalization raises the experimental cross section by $\approx 8\%$.) The two results agree within 7% at $T = 100$ eV. One must go beyond the PWBA to achieve a better agreement with experiment.[24] A by-product of the Bethe cross sections for the Rydberg states (Table III) is the estimate of cascade corrections needed in interpreting the experimental data based on the optical-excitation functions, such as those by Enemark and Gallagher.[23] Our data in Table III indicate that the sum of cross sections for the $n\,^2D$ and $n\,^2S$ excitations at $T = 1003$ eV amounts to $0.103\pi a_0^2$. These values are in good agreement with the cascade correction used in Ref. 23, $0.136\pi a_0^2$.

B. Transitions to higher excited states

Hertel and Ross[25] converted their electron-impact data to the GOS for higher transitions to states such as $n\,^2S$ ($n = 4-6$), $3\,^2D$, $4\,^2D$, $4\,^2F$, and $5\,^2P$. In all cases, we find that the slopes of the "experimental" GOS's for small momentum transfers by Hertel and Ross[25] are two to three times larger than our calculated results (Table VIII). Theoretical slopes by McGuire[13] are in good agreement with our values. The incident energies used in the experiment (< 100 eV) probably are too low

TABLE VII. Bethe parameters for total inelastic scattering, discrete excitation, and ionization cross sections for Fe^{15+}.

	A	B	C
Total inelastic scattering (σ_{tot})	0.278	−0.053	2.68
Sum of discrete excitations (σ_{ex})	0.167	0.165	1.80
Ionization (σ_{ion})	0.111	−0.218	0.88

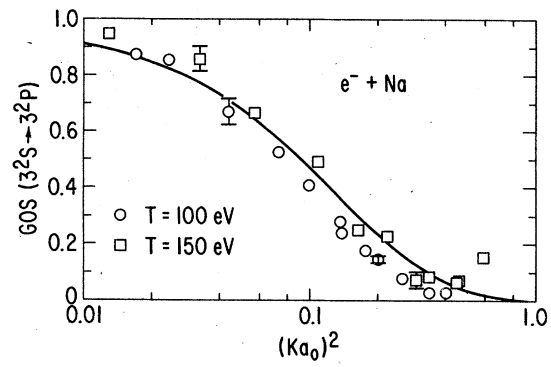

FIG. 8. The generalized oscillator strength for the $3\,^2P$ excitation of Na. Circles and squares represent the "experimental" GOS deduced from the electron-impact data by Shuttleworth *et al.* (Ref. 22) at incident energies of 100 and 150 eV.

to justify the interpretation of the experiment through the Born approximation.

C. Relativistic effects

In Sec. III we already mentioned that relativistic effects reduce the values of A_n and B_n. The effect of the lower values of A_n on σ_n is significant at high incident energies where the logarithmic term in Eq. (4) is sizable. The reduction in B_n, however, reduces σ_n at lower incident energies as well. From Figs. 1–5, we see that the relativistic effects in the ions affect σ_n more in the $^2P_{3/2}$ excitations than in the $^2P_{1/2}$ excitations. For $Z > 40$,

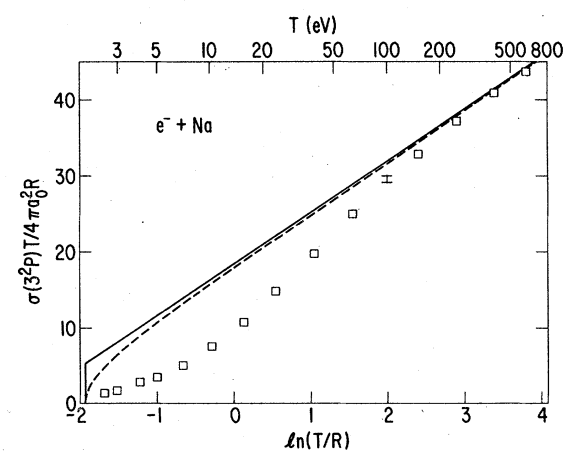

FIG. 9. The Fano plot of the integrated cross section for the $3\,^2P$ excitation of Na. The squares are the electron-impact data by Enemark and Gallagher (Ref. 23). The solid line is the Bethe cross section, Eq. (4), and the broken curve is the Born cross section, Eq. (2), obtained without the Bethe approximation. The experimental uncertainty (e.g., at incident energy $T = 100$ eV) is masked by the size of the squares.

TABLE VIII. Slope of the generalized oscillator strengths for small momentum transfers.

Transition	$\left.\frac{df_n(K)}{d(Ka_0)^2}\right\|_{K=0}$ Experiment[a]	Theory[b]	Present work
$4\,^2S$	0.8 ±0.6	1.4	1.51
$5\,^2S$	0.58 ±0.8	0.20	0.230
$6\,^2S$	0.12 ±0.04	0.074	0.0801
$4\,^2P$	1.9 ±0.6		0.573
$5\,^2P$	0.41 ±0.2		0.114
$3\,^2D$	8.9 ±0.9	2.8	3.16
$4\,^2D$	1.9 ±0.3[c]	0.50	0.550

[a] From Ref. 25.
[b] From Ref. 13.
[c] Reference 25 presents $4\,^2D + 4\,^2F$, but $4\,^2F$ does not contribute to the slope because of a selection rule.

relativistic description of the target should be used even for low incident energies.

D. Ionization of Na

In Fig. 10, we compare our result with electron-impact data by McFarland and Kinney,[9,10] and the PWBA results by Peach,[12] McGuire,[13] and Omidvar *et al.*[14] Peach used analytic Hartree-Fock wave functions for bound electrons and a Coulomb function of unit charge for the ejected electron. McGuire used Herman-Skillman-type wave functions for both bound and ejected electrons. The work by Omidvar *et al.* is similar to that by Peach except for the use of screened hydrogenic functions for bound electrons. The structures seen in the data by Peach and by McGuire are related to the thresholds for inner-shell excitation followed by autoionization.

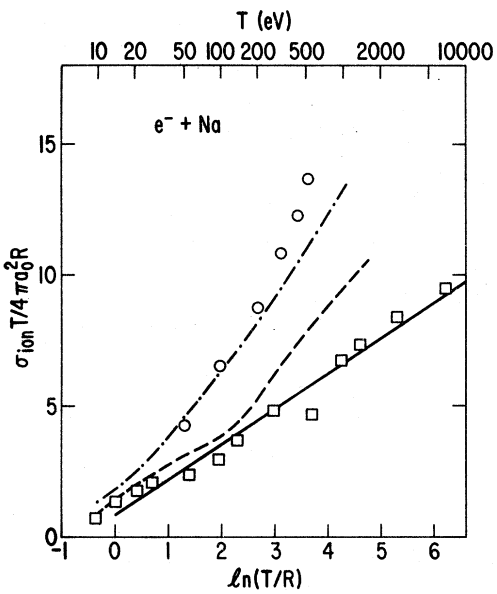

FIG. 10. The Fano plot of the ionization cross section of Na by electron impact. The circles represent the experimental data by McFarland and Kinney (Ref. 9). The squares represent the Born cross section calculated by McGuire (Ref. 13), the broken curve that by Peach (Ref. 12), and the chained curve that by Omidvar *et al.* (Ref. 14). Our Bethe cross section is given by the solid line.

All the PWBA results quoted in Fig. 10 explicitly include contributions from $2s$ and $2p$ electrons. Contributions from the K shell were not included in Refs. 12 and 14, but they are expected to be insignificant. In contrast, the sum-rule method automatically includes both autoionization and direct-ionization contributions from the K and L shells. Therefore, in the asymptotic region, our σ_{ion} must be an upper limit to all data quoted in Fig. 10. We used the revised experimental data from Ref. 10 in Fig. 10. The experimental data are for the production of singly charged ions only, and certainly should be below our data at high incident energies.

From Fig. 10 it is clear that only the PWBA calculation by McGuire[13] is consistent with our result in the asymptotic region. The main difference between the work of McGuire and that of Peach is in the continuum wave function for the ionized electron. Our work indicates that the Coulomb functions with a fixed nuclear charge (bare or screened) will not lead to a realistic ionization cross section in the asymptotic region.

As was suggested by McGuire,[13] the experimental data by McFarland and Kinney[9] should be reduced by about a factor of 2. Furthermore, the upward revision of the experimental data reported by McFarland[10] seems to be an overcorrection.

E. Ionization of Fe^{15+}

Only theoretical data are available for σ_{ion} of Fe^{15+}, those by Rudge and Schwartz,[18] and by Bely.[26] Bely specifically discussed the importance of autoionization following the excitation of the L-shell electrons. Their results are compared with our Bethe cross section in Fig. 11. Below the ionization thresholds of $2s$ and $2p$ electrons indicated in Fig. 11, the sum-rule method is unreliable because only $3s$ electrons can be ionized in reality, whereas our ionization cross section does not eliminate the inner-shell contributions. The Bethe cross section, however, is expected to provide a reliable upper limit for ionization in the asymptotic region beyond the $1s$ threshold. Comparison of the Rudge-Schwartz and Bely results with ours in Fig. 11 shows that the former are a factor of 2–3 smaller than ours in the asymptotic

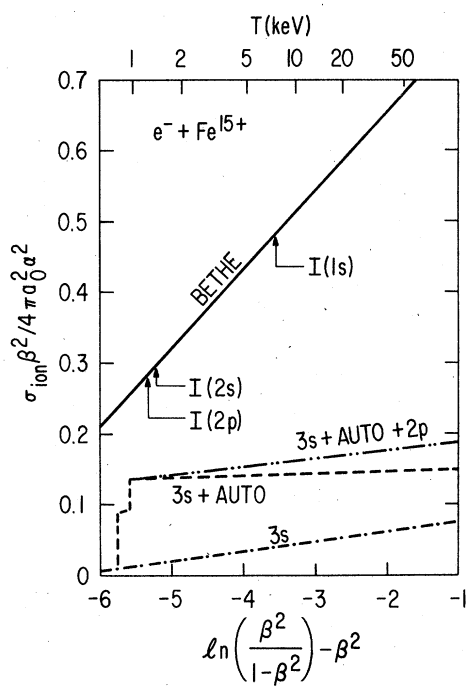

FIG. 11. The Fano plot of the ionization cross section of Fe^{15+} by electron impact. The curve marked 3*s* represents the Coulomb-Born cross section for the direct ionization of the valence electron by Rudge and Schwartz (Ref. 18), the curve marked 3*s* + AUTO includes the autoionization cross section following the excitation of the 2*s* and 2*p* electrons [calculated by Bely, Ref. 26], and the curve marked 3*s* + AUTO + 2*p* includes also the direct ionization of the 2*p* electrons calculated by Rudge and Schwartz (Ref. 18). The solid line is our Bethe cross section. Ionization thresholds of the inner-shell electrons are indicated by $I(nl)$.

region. Even though the *K*-shell contribution is neglected in Refs. 18 and 26, it is unlikely that the 1*s* electrons are responsible for all the difference in the asymptotic region.

As we mentioned in Sec. III, Rudge and Schwartz[18] scaled their cross sections by I^2, where I is the ionization potential. Although the values of I used by them are close to our relativistic Hartree-Fock values, the Z^2 scaling seems to give smoother Z dependence of cross sections.

VI. CONCLUSIONS

Major results obtained in the present work are: (a) the cross sections along the isoelectronic sequence are scaled better by Z^2 rather than by the screened charge or excitation energies, (b) the experimental σ_{ion} of Na by McFarland and Kinney[9] is likely to be a factor of 2 too large, (c) the Born σ_{ion} of Na by McGuire[13] agrees very well with ours, and (d) the σ_{ion} of Fe^{15+} calculated by Rudge and Schwartz,[18] and also by Bely,[26] are far below the Bethe cross section in the asymptotic region.

The slopes of the generalized oscillator strengths of Na at small momentum transfer measured by Hertel and Ross[25] disagree with our calculated results. It is likely that the incident energies (< 100 eV) used by them are too low to interpret their data in terms of the Born approximation.

Two relativistic effects in the target ions, one that reduces the dipole matrix element and the other that increases excitation energy, lower the PWBA cross sections. We recommend that the relativistic description be used for medium and heavy target ions regardless of incident energies, particularly for collision theories that aim at high reliability.

ACKNOWLEDGMENTS

We would like to thank T. Baer for providing us with the value of $L(-1)$ for Fe^{15+}. We are indebted to Dr. J. P. Desclaux for his computer programs to calculate relativistic and nonrelativistic Hartree-Fock wave functions. This work was performed under the auspices of the U. S. Department of Energy.

[1]See, for instance, U. S. Energy Research and Development Administration Report No. ERDA-77-73, 1977 (unpublished).
[2]M. J. Seaton, Adv. At. Mol. Phys. 11, 83 (1975).
[3]H. A. Bethe, Ann. Phys. (Leipz.) 5, 325 (1930).
[4]A. L. Merts, R. D. Cowan, and N. H. Magee, Jr., Los Alamos Scientific Laboratory Report No. LA-6220-MS, 1976 (unpublished).
[5]M. Inokuti, Y.-K. Kim, and R. L. Platzman, Phys. Rev. 164, 55 (1967).
[6]Y.-K. Kim and M. Inokuti, Phys. Rev. A 3, 665 (1971).
[7]J. T. Tate and P. T. Smith, Phys. Rev. 46, 773 (1934).
[8]G. O. Brink, Phys. Rev. 134, A345 (1964).
[9]R. H. McFarland and J. D. Kinney, Phys. Rev. 137, A1058 (1965).
[10]R. H. McFarland, Phys. Rev. 139, A40 (1965).
[11]I. P. Zapesochnyi and I. S. Aleksakhin, Zh. Eksp. Teor. Fiz. 55, 76 (1968) [Sov. Phys. JETP 28, 41 (1969)].
[12]G. Peach, J. Phys. B 3, 328 (1970).
[13]E. J. McGuire, Phys. Rev. A 3, 267 (1971).
[14]K. Omidvar, H. L. Kyle, and E. C. Sullivan, Phys. Rev. A 5, 1174 (1972).
[15]M. Inokuti and Y.-K. Kim, Phys. Rev. 186, 100 (1969).
[16]U. Fano, Ann. Rev. Nucl. Sci. 13, 1 (1963).
[17]J. P. Desclaux, Comput. Phys. Commun. 9, 31 (1975).
[18]M. R. H. Rudge and S. B. Schwartz, Proc. Phys. Soc.

Lond. 88, 579 (1966).
[19]H. A. Bethe and E. E. Salpeter, *Quantum Mechanics of One- and Two-Electron Atoms* (Springer-Verlag, Berlin, 1957), p. 265.
[20]J. L. Dehmer, M. Inokuti, and R. P. Saxon, Phys. Rev. A 12, 102 (1975).
[21]T. Baer, ANL Report No. ANL-77-65, 1977 (unpublished).
[22]J. Shuttleworth, W. R. Newell, and A. C. Smith, J. Phys. B 10, 1641 (1977).
[23]E. A. Enemark and A. Gallagher, Phys. Rev. A 6, 192 (1972).
[24]See, for instance, J. V. Kennedy, V. P. Myerscough, and M. R. C. McDowell, J. Phys. B 10, 3759 (1977).
[25]I. V. Hertel and K. J. Ross, J. Phys. B 2, 285 (1969).
[26]O. Bely, J. Phys. B 1, 23 (1968).